THE JOURNAL OF BIOLOGICAL CHEMISTRY
Vol. 278, No. 6, Issue of February 7, pp. 3929–3936, 2003

Printed in U.S.A.

Reconstitution of Holin Activity with a Synthetic Peptide Containing the 1–32 Sequence Region of EJh, the EJ-1 Phage Holin*

Received for publication, November 6, 2002, and in revised form, December 1, 2002
Published, JBC Papers in Press, December 2, 2002, DOI 10.1074/jbc.M211334200

Amparo Haro,[a,b] Marisela Vélez,[c] Erik Goormaghtigh,[d,e] Santiago Lago,[f] Jesús Vázquez,[g] David Andreu,[h] and María Gasset[a,i]

From the [a]Insto de Química-Física Rocasolano and [g]Centro de Biología Molecular Severo Ochoa, Consejo Superior de Investigaciones Científicas, Madrid 28006, Spain, the [c]Facultad de Ciencias C-XVI, University Autónoma, Madrid 28049, Spain, [d]Structure and Function of Biological Membranes, University Libre Bruxelles, Bruxelles B1050, Belgium, the [f]Facultad Ciencias Experimentales, University Pablo de Olavide, Sevilla 41013, Spain, and the [h]Departamento Ciencias Experimentales y de la Salud, University Pompeu Fabra, Barcelona 08003, Spain

Pneumococcal EJ-1 phage holin (EJh) is a hydrophobic polypeptide of 85 amino acid residues displaying lethal inner membrane disruption activity. To get an insight into holin structure and function, several peptides representing the different topological regions predicted by sequence analysis have been synthesized. Peptides were structurally characterized in both aqueous buffer and membrane environments, and their potential to induce membrane perturbation was determined. Among them, only the N-terminal predicted transmembrane helix increased the membrane permeability. This segment, only when flanked by the positive charged residues on its N-terminal side, which are present in the sequence of the full-length protein, folds into a major α-helix structure with a transmembrane preferential orientation. Fluorescein quenching experiments of N-terminal-labeled peptide evidenced the formation of oligomers of variable size depending on the peptide-to-lipid molar ratio. The self-assembling tendency correlated with the formation of transmembrane pores that permit the release of encapsulated dextrans of various sizes. When analyzed by atomic force microscopy, peptide-induced membrane lesions are visualized as transbilayer holes. These findings are the first evidence for a lytic domain in holins and for the nature of membrane lesions caused by them.

Holin refers to a family of bacteriophage-encoded small hydrophobic proteins (60–145 amino acid residues) that make up the two-component lysis system used by most double-stranded DNA phages to accomplish the release of the progeny at the last stage of the infection (1). These proteins cause nonspecific lethal lesions (holes) of the host cytoplasmic membrane, which allow the passage of the murein hydrolase to the periplasm for proteoglycan degradation (1–3). This ability makes holins the regulators of both the timing of host lysis and the yield of the phage progeny. Despite the increasing number of holin family members described by genetic analysis and their promising use in biotechnology, their structure and molecular mechanism of action are still unknown (2–6).

Most, if not all, of the current knowledge on holins is based on the λ phage S protein, a type I holin characterized by a dual start motif and three potential transmembrane segments (3, 7). Genetic studies have provided the evidences for essential residues and the basis for function regulation. Thus, N- and C-terminal solvent-exposed regions have been proposed as lysis timing regulators, their positive charge content being directly correlated with the onset retardation (8, 9). On the other hand, the hydrophobic segments have been suggested to be responsible for the permeation event, because they contain most of the inactivating mutations (10, 11). In addition, biochemical studies have determined the location of the protein at the inner membrane, verified its predicted helical structure in detergent micelles, and evidenced its permeating properties in model membranes (12, 13). All these data have set the basis for a model in which a homo- or hetero-oligomer of transmembrane helices forms a functional pore (2, 13).

EJh,[1] the holin of the temperate pneumococcal EJ-1 phage, is an 85-amino acid polypeptide chain ascribed to the type II holin subgroup (14). As shown for λS holin, EJh expression is lethal for the host cell (14). In contrast to λS holin, the EJh polypeptide chain lacks a defined dual start, and its sequence analysis only allows the prediction of two transmembrane regions of higher hydrophobicity. To gain insight into the molecular and structural basis of EJh membrane lesions, we have undertaken a fragment approach to the polypeptide chain. The synthetic peptides were conformationally characterized, both in aqueous and in membrane environments, and their capacity to induce membrane leakage was assayed. The body of results revealed the predicted N-terminal transmembrane helix as the potential active region of the holin molecule. When synthesized as a peptide, including the charged N terminus (1–32 sequence seg-

* This work was supported in part by Grants PB96/0850 and BIO2000-1664 of the Ministerio de Ciencia y Tecnologia (to M. G.). The costs of publication of this article were defrayed in part by the payment of page charges. This article must therefore be hereby marked "*advertisement*" in accordance with 18 U.S.C. Section 1734 solely to indicate this fact.

[e] Research Director of the Fonds National de Recherche Scientific (Belgium).

[b] Present address: Biotools BM Laboratories, Valle de Tabalinas 52 N-43, Madrid 28021, Spain.

[i] To whom correspondence should be addressed: Instituto Química-Física Rocasolano, Consejo Superior de Investigaciones Científicas, Serrano 119, Madrid 28006, Spain. Tel.: 34-915-619-400; Fax: 34-915-642-431; E-mail: mgasset@iqfr.csic.es.

[1] The abbreviations used are: EJh, EJ-1 phage holin; EJh-Li and EJh-Mi, synthetic peptides representing the i solvent-exposed and i membrane-spanning predicted regions, respectively; ANTS, aminonaphtalene-3,6,8-trisulfonic acid; DPX, *p*-xylenebis(pyridium bromide); Flu, 5-(and 6)-carboxyfluorescein; FD-70, FD-20, and FD-4, fluorescein isothiocyanate dextrans of 70, 20, and 4 kDa, respectively; POPC, 1-palmitoyl-2-oleoyl-*sn*-glycero-3-phosphocholine; POPE, 1-palmitoyl-2-oleoyl-*sn*-glycero-3-phosphoethanolamine; POPG, 1-palmitoyl-2-oleoyl-*sn*-glycero-3-phosphoglycerol; P:L, peptide-to-lipid molar ratio; LUV, large unilamellar vesicle; TFE, 2,2,2-trifluoroethanol; CD, circular dichroism; ATR-FTIR, attenuated total reflection Fourier transform infrared; AFM, atomic force microscopy.

ment), this region folded into a transmembrane helix displaying self-assembly properties that permit membrane permeation to dextrans of various sizes. Finally, the study of peptide-induced bilayer lesions by atomic force microscopy has allowed the visualization of polydisperse defects as holes. To the best of our knowledge this is the first report on the nature of lytic domain and the bilayer lesions carried out by holins.

EXPERIMENTAL PROCEDURES

Chemicals—Protected amino acids, resins, and other peptide synthesis reagents were from Bachem. All lipids were purchased from Avanti Polar Lipids. ANTS, DPX, Flu, and Flu succinimidyl ester were purchased from Molecular Probes. D_2O (99.9% isotopic enrichment), FD-4, FD-20, and FD-70 were obtained from Sigma-Aldrich. Sephadex G-75 and Sephacryl S-300 were purchased from Amersham Biosciences. All reagents for buffer preparation and other experimental procedures were of the highest commercial quality.

Peptide Synthesis and Purification—EJh peptides were synthesized using standard solid-phase methods with either Fmoc (*N*-(9-fluorenyl)-methoxycarbonyl) (15) or *tert*-butyloxycarbonyl (16) chemistry. Flu labeling on the N terminus of the resin-bound peptides was performed as previously described (17). Peptides were purified by reverse-phase high-performance liquid chromatography (>97% pure, except about 89% for EJh-M2), and their molecular masses were confirmed by mass spectrometry (18). Water-soluble peptides were extensively dialyzed against 25 mM Hepes-HCl, pH 7.0, buffer containing 0.1 M NaCl and 0.5 mM EDTA using 500-kDa cutoff dialysis tubing and kept frozen. For CD experiments NaCl was replaced by KF. Hydrophobic peptides were first washed with 10 mM HCl, then dissolved in TFE and aliquoted. When required, TFE was evaporated under N_2 stream, and the solid peptide was redissolved in Me_2SO. Peptide concentrations were determined by quantitative amino acid analysis performed at the Protein Chemistry Facility of the Centro de Investigaciones Biológicas.

Liposome Preparation and Complex Formations—Vesicles were prepared by hydration of lipid dry films in 25 mM Hepes-HCl, pH 7.0, containing 0.1 M NaCl and 0.5 mM EDTA, followed by five freeze-thaw cycles and extrusion through polycarbonate membranes of 0.1-μm pore diameter (18). The lipid concentration was determined by phosphorus assays (19). Lipid-peptide complexes were formed by external addition of the peptides to the liposome suspensions. For hydrophobic peptides, peptides were added from a TFE stock solution (final TFE < 0.2%, v/v) except for permeability assays and AFM analysis in which Me_2SO stock solutions were used to avoid membrane damage.

Circular Dichroism—CD spectra were recorded in a Jasco 810 spectropolarimeter at 25 °C (20). The measurements were performed using samples of 0.07–0.2 mM peptide concentration and 0.1-cm path length cells. Spectra are reported as averages of seven scans recorded at a scan rate of 0.33 nm/s. After base line correction and noise reduction the observed ellipticities were converted to mean residue ellipticity in units of degree·cm^2·(decimoles of amino acid residue)$^{-1}$ using the molecular weight per residue calculated from the sequence with ExPASy Tools. The secondary structure composition was determined from the best fit using the least-square fitting methods provided by Jasco and by DICROPROT software. The best fit was considered in terms of goodness of experimental spectrum reproduction with the resulting evolvent and of converge between different fitting methods.

Infrared Spectroscopy—ATR-FTIR spectra were recorded in a Bruker IFS-55 FTIR spectrometer equipped with a nitrogen-cooled mercury cadmium telluride detector and continuously purged with dried air. The internal reflection element was a germanium ATR plate (50 × 20 × 2 mm) tilted 45° relative to the incident beam. For each spectrum, 256 scans at 2 cm^{-1} nominal resolution were averaged. Samples were prepared by slow evaporation of the analyte solution (peptides, lipids, peptide-lipid complexes) under nitrogen stream on one side of the germanium plate and then sealed in a universal sample holder. Isotopic exchange (hydrogen/deuterium) was allowed for 1 h under a stream of nitrogen saturated with heavy water, before spectrum acquisition. Solvent and water vapor absorptions were compensated for by subtracting the respective spectra. Secondary structure analyses of the peptides in the absence and presence of phospholipids were performed as described previously (21). The determination of the molecular orientation was estimated from the linear dichroic spectrum using a KRS-5 polarizer mount assembly (22, 23). The dichroic spectrum is the difference between the spectra recorded with parallel and perpendicular polarizations. The perpendicular spectrum was multiplied by a factor for zeroing the carbonyl-stretching band (1750–1700 cm^{-1}). A larger absorbance for the parallel polarization (positive amide I′ band) of an α-helix indicates a dipole oriented preferentially near the normal of the ATR plate (23). Conversely, a larger absorbance for the perpendicular polarization (positive amide I′ band) of a β-sheet might indicates its preferential orientation parallel to the ATR plate (24).

Fluorescence Spectroscopy—All fluorescence emission measurements were performed on an SLM-8100 spectrofluorimeter at 25 °C, unless otherwise stated. Conventionally, quartz cells (0.5 × 0.5 or 1 × 1 cm) and Glan-Thompson polarizers in magic angle configuration were used. In quenching experiments, Flu-labeled peptide was mixed in TFE with increasing amounts of unlabeled peptide and then added to POPG:POPE (70:30) suspensions at 1:100 and 1:1000 final P:L (0.05–0.1 μM Flu-labeled peptide final concentration). After an overnight incubation at 25 °C, the emission spectra (480-nm excitation wavelength) were recorded before and after the addition of 0.1% SDS. Detergent lysis was used to correct for the slight deviations in concentration. Spectra were corrected for base line and instrument and optical factors. Parallel experiments with POPC vesicles excluded effects of changes in the ionization state of fluorescein on the emission intensities.

Membrane Permeability Assays—Disruption of the membrane permeability barrier was measured using the ANTS/DPX leakage assay (25). Briefly, LUVs were prepared in 10 mM Hepes-HCl, pH 7.0, containing 12.5 mM ANTS, 45 mM DPX, 20 mM NaCl, and 1 mM EDTA and then separated from non-encapsulated material on Sephadex G-75 using 10 mM Hepes-HCl, 0.1 M NaCl, 1 mM EDTA, pH 7.0, as elution buffer. The fluorescence intensity increase of vesicle solution (60–70 μM phospholipid concentration) upon peptide addition was measured through an OG-550 Schott cutoff filter (>530 nm) upon excitation at 386 nm. The 0 and 100% levels of leakage were taken as the intensities of the corresponding vesicle suspension before and after addition of Triton X-100 (0.5% final concentration), respectively. Pore size determination was performed as described (26). Briefly, POPG:POPE (70:30) lipid films were hydrated in 10 mM Hepes-HCl, pH 7.0, 20 mM NaCl, and 1 mM EDTA containing either 3 mg/ml FD-20 and 2 mg/ml FD-4 or 4 mg/ml FD-70 and 0.5 mg/ml Flu, then frozen and thawed 20 times and extruded through 0.2-μm pore diameter membranes. Untrapped dextrans were removed by gel filtration using Sephacryl S-300 HR packed into a 17 × 0.7-cm column and equilibrated in 10 mM Hepes-HCl, pH 7.0, containing 70 mM NaCl and 1 mM EDTA (elution buffer). Fluorescein derivative-containing LUVs were then incubated for 2 h at 37 °C in the absence or presence of 0.5% Triton X-100 and EJh-L1M1 at 1:1500 and 1:750 P:L molar ratio. The treated LUVs were loaded onto a Sephacryl S-300 HR 37 × 1.2-cm column run at 19.8 ml/h in elution buffer. Fractions of 0.5 ml were collected, and their fluorescence emission intensity at 520 nm (480-nm excitation wavelength) was measured. The area under each peak was determined from the analysis of the elution profiles using a three-peak log·normal distribution with Origin 5.0 software.

Atomic Force Microscopy of Supported Bilayer Preparations—POPG and POPG:POPE (70:30) liposomes, prepared by extrusion through polycarbonate membranes of 0.2-μm pore diameter, were incubated in the absence and presence of EJh-L1M1 at a 1:300 P:L molar ratio. The supported membranes were prepared by depositing 50 μl of 1 mg/ml solution of liposomes in 20 mM Hepes-HCl, pH 7.0, containing 0.1 M NaCl and 20 mM $CaCl_2$ on top of freshly cleaved circular pieces of mica glued onto a Teflon surface (27). The liposomes were allowed to fuse on the mica for 30–60 min at room temperature and then extensively washed with buffer. AFM images were taken with an Atomic Force microscope (Nanotec Electronica, Madrid, Spain) operated in the contact or jump mode (28, 29). Silicon nitride tips with a force constant of 0.12 newtons/m (DI instruments) were used. The samples were maintained under buffer solution while imaging. The number of peptide molecules constituting a hole was estimated from the linear packing of spheres of an α-helix-like radius (0.5 nm) in the perimeter of the lesion. The number of lipid molecules was estimated considering a lipid head group area of 65 Å^2 (30).

RESULTS

EJh Sequence as Template for Peptide Design—Hydropathy profiles of EJh polypeptide chain predicted the presence of three solvent-exposed regions and two hydrophobic segments compatible with membrane-spanning α-helices (14). This structural trend would sustain the folding of the polypeptide chain as a transbilayer helix-turn-helix that could hypothetically act as a scaffold unit for the formation of an oligomeric assembly displaying membrane-permeating properties (Fig. 1). In the context of this model, at least two types of active oligomers

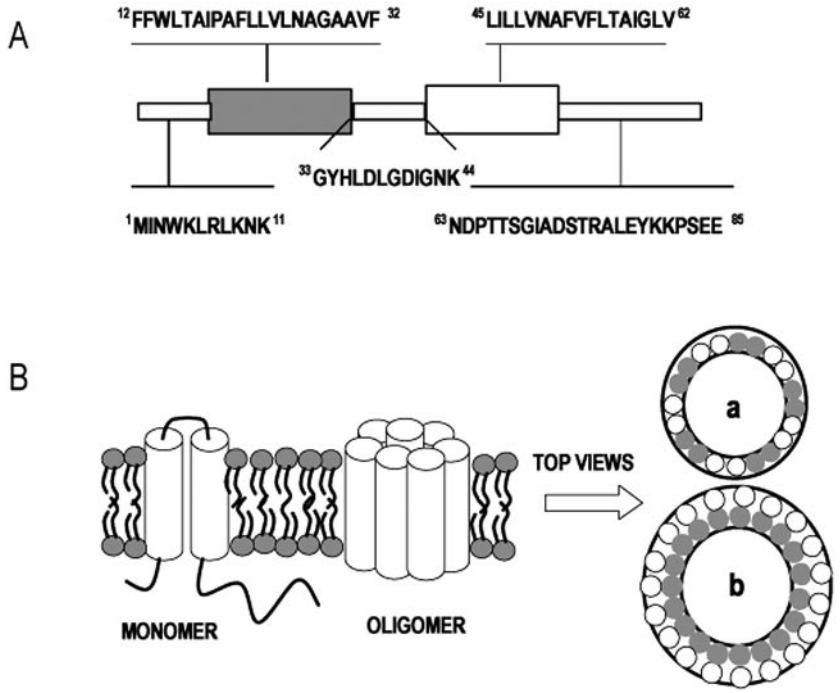

FIG. 1. **EJh sequence, predicted folding, and hypothetical models for its biological action.** *A*, EJh sequence as template for peptide synthesis following the hydrophobic analysis previously performed (14). Regions predicted as putative transmembrane regions are depicted as *thick rectangles*. *B*, folding model for EJh molecule assuming a two transmembrane α-helix scaffold for oligomerization (2). *Top views* of the possible oligomeric structures. Model *a* involves a heterogeneous pore wall made of both transbilayer segments. Model *b* involves a homogeneous pore wall (*a priori* either *gray* or *white segments* would be consistent with the model).

TABLE I
Major secondary structure of EJh-based peptides

The secondary structure composition was determined by analysis of CD and ATR-FTIR spectra as described under "Experimental Procedures." The structure indicated is that which the peptide populates to at least 40%. In CD experiments, *aqueous buffer* refers to both 20 mM Hepes-HCl, pH 7.0, containing 0.1 M KF, 0.5 mM EDTA, and 20 mM phosphate, pH 7.0. For ATR-FTIR, spectra were collected in peptide films obtained from 10 mM Tris-HCl, pH 7.0, initial solutions, except in the case of EJh-M1 and EJh-M2 where the transfer was carried out from 40% TFE solutions. Membranes refer to the presence of POPG:POPE (70:30) at a 1:10 P:L molar ratio.

Peptide	Sequence	Aqueous buffer		Membranes	
		CD	ATR-FTIR	CD	ATR-FTIR
EJh-L1	^{1}MINWKLRLKNK^{11}	Random	Random plus β-sheet	ND[a]	β-Sheet
EJh-M1	^{12}FFWLTAIPAFLLVLNAGAAVF^{32}	β-Sheet	β-Sheet plus random	α-Helix	α-Helix
EJh-L2	^{33}GYHLDLGDIGNK^{44}	Random plus turn	Random plus turn	Random plus turn	Turn plus random
EJh-M2	^{45}LILLVNAFVFLTAIGLV^{62}	Insoluble	Turn plus β-sheet	Insoluble	Turn plus β-sheet
EJh-L3	^{63}NDPTTSGIADSTRALEYKKPSEE^{85}	Random	Random	Random	Random plus turn

[a] The turbidity of the sample precluded the spectrum registration below 210 nm. ND, not determined.

differing in the nature of the transmembrane segment forming the aqueous cavity can be considered. To elucidate the secondary structure and the molecular basis of membrane permeation, the EJh chain was chemically synthesized as different individual fragments (Table I and Fig. 1).

Secondary Structure of EJh Peptides—The secondary structure of EJh-based peptides was probed by both far-UV CD and ATR-FTIR spectroscopies in aqueous and membrane environments (Figs. 2 and 3 and Table I). In aqueous buffers, EJh-L1 and EJh-L3 displayed CD spectral features of mainly nonordered conformations. Under similar conditions, EJh-L2 spectral shape revealed the coexistence of both turns and nonordered conformations. In the three cases, spectral analysis by least-square fitting supported the previous structural trend, even though the contribution from non-amide chiral components arising from Trp and Tyr chains was not considered (31, 32). When inspected by ATR-FTIR, amide I′ band analysis also confirmed the conformational trend for EJh-L2 and EJh-L3 but clearly revealed the presence of β-sheet structure (peak at 1628 cm^{-1}) in EJh-L1 (Fig. 3*A*). EJh-M1 and EJh-M2, both representing the predicted transmembrane regions, displayed limited solubility in aqueous buffer. Dilution of the peptides from TFE stock solutions into aqueous buffers revealed the formation of extended structures, which were soluble in the case of EJh-M1 but insoluble in the case of EJh-M2 (Fig. 2). When analyzed by ATR-FTIR as films dried from 40% TFE solutions, the amide I′ band of EJh-M1 suggested a helix-random mixture, whereas that of EJh-M2 revealed signatures of turn (1675 cm^{-1}) and β-sheets (1628 cm^{-1}) (Fig. 3*A*).

In the presence of POPG:POPE (70:30) vesicles (1:10 P:L to avoid light scattering interference), the CD spectra of both EJh-L2 and EJh-L3 remained unchanged (data not shown). The ATR-FTIR spectra agree with the corresponding CD spectra, and underline the preference of EJh-L2 for adopting a turn structure as evidenced from the band at 1675 cm^{-1} (Fig. 3*B*). In contrast to the previous cases, addition of POPG-containing vesicles to EJh-L1 caused the appearance of a negative band in the CD spectrum and an increase in resolution of the amide I′ band compatible with β-sheet structures (Fig. 3*B*). Furthermore, the linear dichroism ATR-FTIR spectrum of lipid-bound EJh-L1 revealed a negative band characteristic of extended structures lying parallel to the membrane surface (Fig. 3*C*). In the presence of membranes EJh-M1 exhibited spectral features typical of helical structures (a major narrow amide I′ band centered at 1655 cm^{-1}) but lacking a preferential orientation with respect to the lipid bilayer as judged by the flat linear dichroism ATR-FTIR spectrum. On the contrary, the spectral signatures of EJh-M2 in the presence of both membranes and SDS micelles supported a complex mixture of turn and β-sheet structures. Larger versions of EJh-M2, such as DIGNK-

EJh-M2 and EJh-M2-NDPT, designed to increase net peptide charge, did not change the conformational features (data not shown).

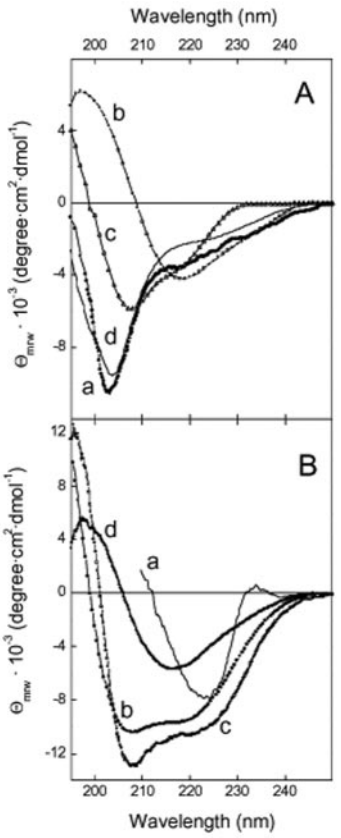

FIG. 2. **Far-UV CD spectra of EJh peptides in aqueous and membrane environments.** *A*, CD spectra in aqueous buffer of: *a*, EJh-L1; *b*, EJh-M1; *c*, EJh-L2; and *d*, EJh-L3. EJh-M2 precipitated, and its spectrum is not shown. *B*, CD spectra of: *a*, EJh-L1 in the presence of POPG:POPE (70:30), EJh-M1 in the presence of POPG:POPE (70:30) (*b*) and SDS micelles (*c*), and EJh-M2 in the presence of SDS micelles (*d*). The CD spectra of EJh-L2 and Ejh-L3 in the presence of POPG:POPE membranes were similar if not identical to *traces c* and *d* of *A*, respectively. Peptide concentrations were about 0.05–0.1 mM. POPG:POPE (70:30) vesicles were used in a 10:1 L:P molar ratio. Aqueous buffer refers to 20 mM Hepes-HCl, pH 7.0, containing 0.1 M KF and 0.5 mM EDTA, although similar results were obtained in 20 mM phosphate, pH 7.0. SDS micelles refers to 17 mM SDS in 20 mM phosphate, pH 7.0.

Taken together these results indicated that the EJh polypeptide chain can be described, from the N terminus to the C terminus, by: (i) an 11-residue segment that distributes between a non-ordered aqueous phase and a membrane-bound β-sheet; (ii) a 22-residue segment folded into a helix structure; (iii) a segment that folds into a membrane-stabilized turn structure; (iv) a second hydrophobic region that collapses into a β structure; and (v) a non-ordered C-terminal tail. This structural trend is in good agreement with the prediction analysis, except for the β-sheet-forming tendencies of both EJh-L1 and EJh-M2. In the case of EJh-L1 the formation of β-sheet structures upon acidic lipid binding can be explained by the i, i+2 amphipathicity of its sequence. On the other hand, EJh-M2 behavior can be explained in terms of the absence of regulatory long range interactions as previously described for other helical segments when handled as isolated peptides (33–35).

Membrane Permeabilization Activity of EJh-based Peptides—Once EJh fragments were structurally characterized we addressed their capacity to produce membrane lesions on ANTS-DPX-loaded vesicles (25). Co-encapsulation of ANTS probe with DPX extinguishes its fluorescence, which, if released to the medium, increases due to dequenching upon DPX dilution. Among all peptides tested, only EJh-L1 and EJh-M1 were capable of inducing an increase in ANTS fluorescence compatible with a membrane lesion event (Fig. 4).

Using either POPG:POPE (70:30) or POPG:POPC (70:30), the ANTS fluorescence relief induced by EJh-L1 was fast and saturated at about 1:10 P:L molar ratio. On the contrary, the vesicle leakage produced by EJh-L2 followed biphasic kinetics compatible with the existence of two steps, a fast membrane insertion and a slow in-membrane oligomerization event (Fig. 4*A*). In this case, end-point titrations at 60 min revealed that saturation of probe release after 1 h of incubation was achieved at a P:L ratio of 1:1000 (Fig. 4*B*). This latter figure must be taken cautiously, because increasing the peptide concentration in solution can favor the formation of peptide aggregates noncompetent for leakage. In fact, the lack of leakage completion at increasing peptide concentrations might support side reactions involving peptide aggregation in aqueous media that would decrease the yield of the membrane interaction process.

Fig. 4*C* shows the lipid composition dependence of EJh-L1- and EJh-M1-induced vesicle leakage. EJh-L1-perturbing activity highly depended on the acidic lipid content of the target membrane, with the maximum leakage being observed for pure POPG vesicles. For this lipid, leakage was accompanied by a

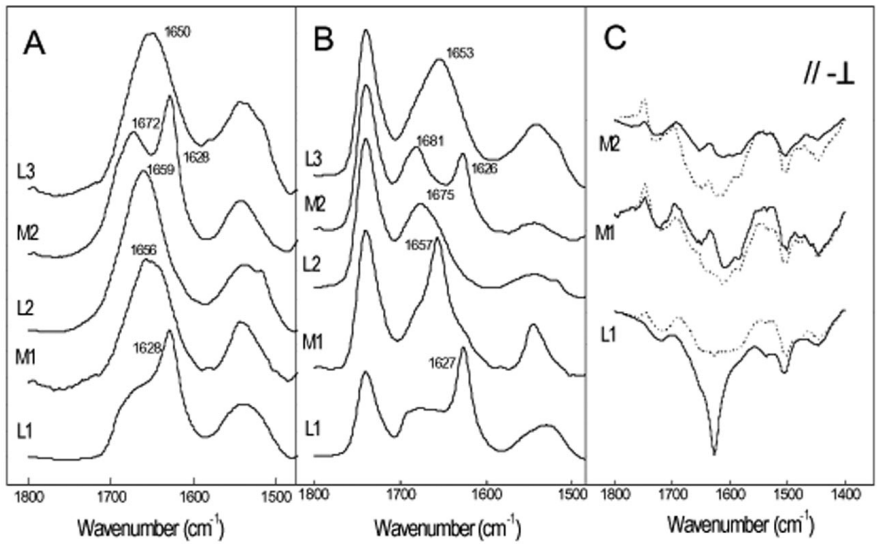

FIG. 3. **ATR-FTIR spectra of EJh peptides in both aqueous solutions and membranes.** *A*, ATR-FTIR spectra of lipid free (from *bottom* to *top*) EJh-L1, EJh-M1, EJh-L2, EJh-M2, and EJh-L3. EJh-L1, EJh-L2, and EJh-L3 were dried on the Ge crystal from 10 mM Tris-HCl solutions with the pH adjusted to 7.0. EJh-M1 and EJh-M2 were dried from solutions prepared in 40% TFE. *B*, ATR-FTIR spectra of (from *bottom* to *top*) EJh-L1, EJh-M1, EJh-L2, EJh-M2, and EJh-L3 in the presence of POPG:POPE (70:30) membranes at a 10:1 lipid-to-peptide molar ratio. Samples were prepared by mixing the required amounts of lipid vesicles and peptides. EJh-Li peptides were added from aqueous stock solutions, whereas EJh-Mi and EJh-L1M1 peptides were prepared in 40% TFE. *C*, linear dichroic ATR-FTIR spectra of EJh-L1, EJh-M1, and EJh-M2 complexed with POPG (*solid*) and POPG:POPE (70:30) (*dotted*) membranes at a 10:1 lipid-to-peptide molar ratio.

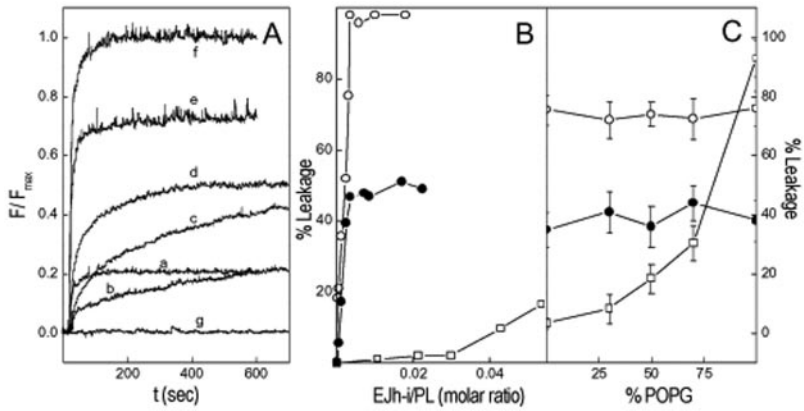

FIG. 4. **Effect of EJh peptides on lipid vesicle permeability assessed by ANTS-DPX dequenching leakage assay.** *A*, kinetics of ANTS fluorescence dequenching by co-encapsulated DPX in POPG:POPE (70:30) vesicles. Depicted traces correspond to: (*a*) EJh-L1 at 1:10 P:L; EJh-M1 at (*b*) 1:1000, (*c*) 1:100 and (*d*) 1:50 P:L; EJh-L1M1 at (*e*) 1:1000 and (*f*) 1:100 P:L; (*g*) peptide-free lipid vesicles. Traces obtained upon addition of EJh-L2, EJh-M2, and EJh-L3 are superimposed on *trace g*. *B*, percentage of leakage from POPG:POPE (70:30) vesicles induced by EJh-L1 (*open squares*), EJh-M1 (*solid circles*), and EJh-L1M1 (*open circles*) as a function of P:L molar ratio. *C*, variation of vesicle leakage with the membrane POPG content: EJh-L1 at 1:10 P:L (*open squares*), EJh-M1 at 1:100 P:L (*solid circles*), and EJh-L1M1 at 1:100 P:L (*open circles*). Displayed data correspond to POPG:POPE mixtures, but those made of POPG:POPC yielded identical results.

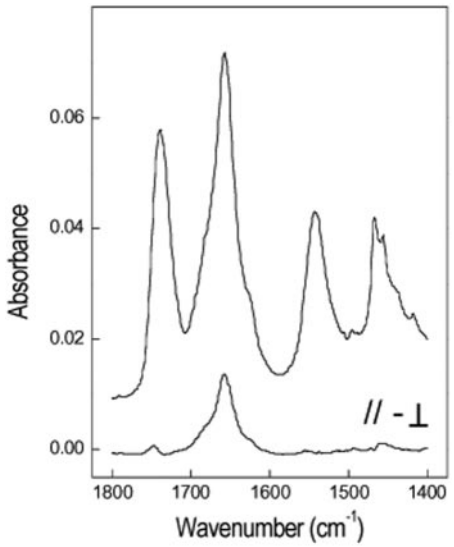

FIG. 5. **ATR-FTIR analysis of EJh-L1M1 secondary structure and membrane orientation.** EJh-L1M1 was incorporated into POPG:POPE (70:30) vesicles at 1:10 P:L, dried on the Ge plate and subjected to hydrogen/deuterium exchange for 1 h (*upper spectrum*). The linear dichroism ATR-FTIR spectrum was calculated as described under "Experimental Procedures."

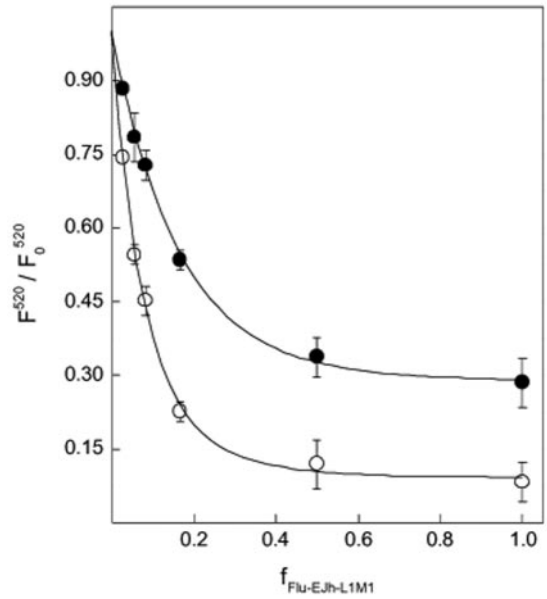

FIG. 6. **EJh-L1M1 oligomerization in membranes followed by the self-quenching of fluorescein-labeled peptide.** Mixtures of Flu-labeled and unlabeled EJh-L1M1 were incubated with POPG:POPE (70:30) vesicles at 1:100 and 1:1000 P:L, and the fluorescence intensity at 520 nm was taken from the emission spectra. Flu-EJh-L1M1 concentration was kept in the 0.05–0.1 μM range. Quenching was calculated as F^{520}/F_0^{520} ratio, where F^{520} and F_0^{520} are the fluorescence intensities of Flu-labeled peptide at a given molar fraction and at infinite dilution, respectively. F_0^{520} was obtained from the fit of the experimental data. Displayed data are the average of two independent measurements.

dramatic increase in solution turbidity (data not shown), suggesting that the permeability perturbation occurs as a consequence of a major liposome membrane rearrangement. Decreasing POPG content in the target vesicle decreased the leakage extent to a negligible value that made EJh-L1 activity incompatible with lytic activity at the cellular level unless a segregation of acidic lipids is assumed. Contrary to EJh-L1, EJh-M1-induced leakage was independent on the lipid composition of the target vesicle. This feature made EJh-M1 the candidate for housing the hole formation capacity of the entire molecule. It should be emphasized that EJh-L2, EJh-M2, and EJh-L3 did not cause any change in a variety of modifications of the assay, including lipid composition, pH, ionic strength, and temperature.

EJh-L1M1 as a Miniholin Model: Oligomer Assembly and Pore Sizing—In light of the previous results, EJh-M1 fulfilled the secondary structure and functional criteria to be considered the holin domain of the EJh molecule. However, the absence of a preferential orientation with respect to the membrane is puzzling. We considered therefore a longer synthetic peptide, EJh-L1M1, consisting of the natural tandem of EJh-L1 and EJh-M1 (Table I and Fig. 1). In the presence of POPG-containing membranes, EJh-L1M1 folded into a major helical structure as judged by the narrow amide I′ band at 1657 cm^{-1} (Fig. 5). Analysis of the structure composition by amide I′ band resolution enhancement methods resulted in a 46% α-helix, 22% β-sheet, 17% turn, and 15% random structure estimated for different lipid composition (POPG:POPE (70:30) and POPG:POPC (70:30)) and P:L molar ratios (1:10 and 1:100). This similarity allowed us to minimize the contribution from different peptide populations over the secondary structure of a single polypeptide chain. Furthermore, the linear dichroism ATR-

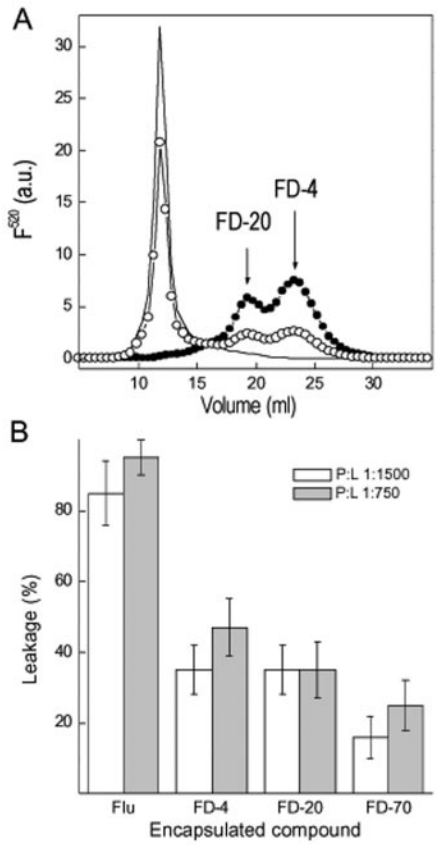

FIG. 7. **Sizing the membrane lesion induced by EJh-L1M1 by gel filtration chromatography.** *A*, typical elution profile of POPG:POPE (7:3) vesicles containing co-encapsulated FD-20 and FD-4, followed by fluorescein emission (F^{520}) as a function of elution volume. Displayed traces correspond to: untreated vesicles (*solid line*), vesicles treated with EJh-L1M1 at 1:1500 P:L (*open circles*), and vesicles lysed with 0.5% Triton X-100. *B*, percentage of leakage of Flu, FD-4, FD-20, and FD-70 from POPG:POPE (70:30) containing co-encapsulated FD-4/FD-20 and Flu/FD-70 mixtures upon incorporation of EJh-L1M1 at the indicated P:L. Column runs were performed in sequential duplicates using the following order: lipids, lipids plus peptide at 1:1500, lipids plus peptide at 1:750, and lipids plus Triton. Percentage of leakage was calculated from the area under each peak and is referenced to the area of the peaks after detergent lysis.

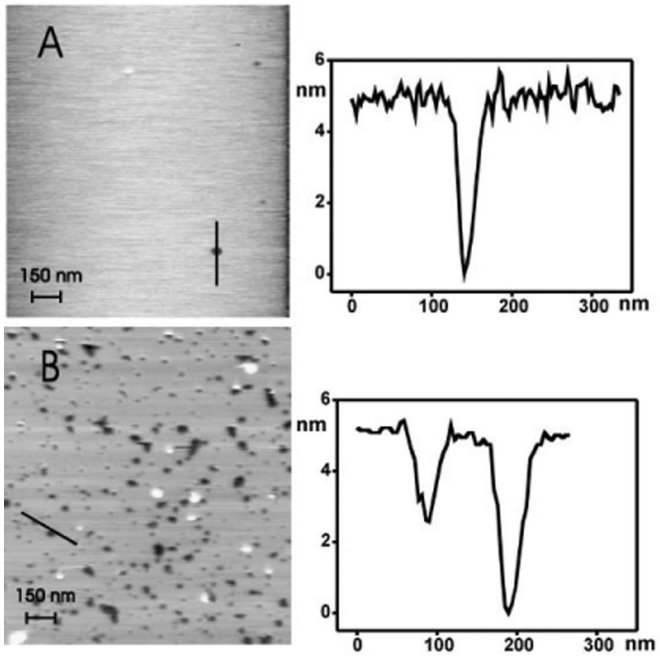

FIG. 8. **AFM images of EJH-L1M1 incorporated into POPG-containing bilayers.** *A*, POPG bilayers fused onto mica; *B*, POPG bilayers containing EJh-L1M1 at a 1:300 P:L and fused onto mica. The *horizontal bar* represents 150 nm. The depth profiles, depicted at the *right-hand side* of each *panel*, correspond to the *dark lines* shown on the *images*. The *total gray scale* represents 10 nm.

FTIR spectrum showed a positive band in the amide I′ region centered at 1657 cm^{-1} (Fig. 5), revealing that the helical structure in EJh-L1M1 is oriented mainly with its axis parallel to the bilayer normal. With regard to membrane-damaging activity, the ANTS-DPX leakage assay showed that EJh-L1M1 retains the membrane-permeating properties of EJh-M1 but with a faster kinetics (Fig. 4).

To test the assembly properties of EJh-L1M1, we used fluorescence quenching experiments (Fig. 6). The experiments were performed using peptide solutions containing a fixed concentration of Flu-labeled and increasing amounts of unlabeled EJh-L1M1 and POPG:POPE (70:30) vesicles. Fluorescence emission at 520 nm diminished with the increase of Flu-EJh-L1M1 molar fraction indicating the existence of an in-membrane oligomerization process. These oligomers were not resistant to detergents, because the addition of SDS or β-octyl glucoside (0.1–1%, w/v final concentration) reverted the fluorescence decreases to a value that was independent of Flu-EJh-L1M1 (data not shown). Furthermore, for a given molar fraction of fluorescent peptide, the extent of quenching was dependent on the total P:L, suggesting that oligomeric species exhibit polydispersity in size.

To get an idea of the pore size we followed a procedure developed by Ladhokin *et al.* (26) that allows simultaneous measurement of the leakage of fluorescein derivatives of different sizes. Fig. 7*A* shows that incubation of EJh-L1M1 at a P:L of 1:1500 with vesicles (200-nm average diameter) containing co-encapsulated FD-4 and FD-20 resulted in the spilling to the medium of both dextrans to an equal extent (35 ± 7%). Under similar conditions, the leakage of co-encapsulated FD-70 and Flu differed notably. The spilling of Flu was almost complete (85 ± 9%), whereas the leakage of FD-70 amounted to only 17 ± 6% (Fig. 7*B*). Increasing the amount of incorporated EJh-L1M1 enhanced the extent of leakage of the encapsulated compounds, suggesting the existence of pores of various sizes. The compromise between assay sensitivity and peptide incorporation under conditions preserving vesicle integrity precluded the study of higher P/L molar ratio. With the available data, and assuming dextrans as prolate ellipsoids of 20-Å short and 40- to 440-Å long axes and a fluorescein hydrodynamic radius of about 6 Å, the permeabilization data suggested a maximum diameter of 25–30 Å (26, 37). Membrane lesions of such size would allow the spill to the medium of Flu and the escape of the dextrans through a slippery mechanism.

To assess the size distribution of membrane lesion we obtained their image with AFM (Fig. 8). Lipid vesicles of various compositions (POPG, POPG:POPC (70:30)) in the absence and presence of EJh-L1M1 (externally added from an Me_2SO stock solution) were fused onto freshly prepared mica surfaces using Ca^{2+} as fusogen (27). Pure lipid bilayers, regardless of composition, were observed as smooth surfaces with statistically negligible defects (Fig. 8*A*). These defects allowed an estimate of 5–6 nm for the thickness of the bilayer plus the water layer between the support and the contact leaflet, in agreement with previously reported data (27, 38). In contrast, when the lipid-peptide assemblies were fused onto the mica, the formed bilayers displayed numerous holes of different sizes, shapes, and depths. Fig. 8*B* illustrates the typical aspect of the surface of a fused POPG:POPC (70:30) bilayer containing EJh-L1M1 at a 1:300 P:L molar ratio. This selected field was fully reproducible

with other lipid compositions except for the heterogeneity of the observable lesions. The holes ranged in diameter from 3 to 44 nm. Their depth was also variable, the largest being as deep as the bilayer and the smallest ones shallower. Given that the diameter of some of the smaller holes was of the same order of magnitude as the expected radius of the tip (10 nm), we could rule out that in those cases the depth measured was limited by the access of the tip into the hole. Therefore, EJh-L1M1 generated membrane lesions of polydisperse size.

A quantitative analysis of the perimeter of the observed holes indicated that the amount of peptide expected to be present in the membrane at the P:L molar ratio used would be enough to line only a third of the perimeter of the total amount of holes observed. This unexpected observation suggested that the presence of EJh-L1M1 transbilayer pores on the liposomes affects the bilayer upon fusion on the mica allowing the enlargement of the defects detected as smaller and shallower holes through the inclusion of peptide-free lipid edges.

DISCUSSION

Genetic studies have provided evidence for the existence of a growing family of phage-encoded small hydrophobic proteins named holins, which are tailored for causing nonspecific membrane lesions (3, 7, 39). These lesions have always been thought as membrane holes but their nature was unknown. The simple constitution of holins as either two or three potential transmembrane helical segments, and the exchangeability of those segments in chimeric molecules, prompted the elaboration of a model in which a protein oligomer is fully responsible for the formation of a membrane pore (7). This in-membrane oligomerization process is particularly important, because it has been correlated with the requirement of a critical mass action pool of protein in the membrane that it is achieved along the lysis timing period (39, 40).

EJh, the holin of the temperate pneumococcal EJ-1 phage is one of the best conserved members of the type-II holin group (7, 14). In contrast to λS, the EJh sequence does not allow the existence of two translation initiation sites (two-start motif) and the consequent activity regulation by the polypeptide chain length (7, 14). Moreover, EJh sequence contains only two hydrophobic regions, whereas λS displays three (7, 14). This apparent simplicity makes EJh an adequate candidate to approach holins in molecular terms.

Theoretical analysis of the EJh sequence predicts the existence of two hydrophobic segments with a length compatible with transmembrane helices separated by a putative turn that permits a minimal helix-turn-helix folding with both chain ends projected into the cytoplasmic side of an imaginary inner membrane (14). All these topological regions, when synthesized as individual peptides and studied by CD and ATR-FTIR spectroscopies, in both aqueous and membrane environments, essentially reproduced the predicted tendencies except in three aspects. First, EJh-L1 (the 11-amino acid N-terminal region) displays an environment-sensitive secondary structure characterized by the stabilization of an extended conformation in the presence of acidic lipids that can be explained on the basis of its sequence amphipathicity. Second, the second predicted transmembrane helix, EJh-M2, collapses into extended aggregates even in the presence of SDS micelles. Extending the chain length with four or five N- and/or C-terminal flanking residues from the protein sequence, and changing the acyl chain of the target membrane has no impact on the observed behavior, thus excluding hydrophobic mismatching effects and solubility impairments. This discrepancy between the theoretical and experimental secondary structure propensity of the isolated EJh-M2 might arise from the dependence of folding on long range interactions, as suggested for other membrane-spanning sequences (33–35, 41). Third, the transbilayer disposition of the first transmembrane region is achieved only in a longer form containing charged amino acids. Therefore, we can conclude that, with the limitations imposed by the absence of long range interaction and the sequential amphiphilicity, the EJh molecule might fold essentially as predicted.

In the quest for finding the polypeptide region responsible for the membrane-damaging activity we tested the previous peptides in a conventional leakage assay. Among them, only those peptides containing the N-terminal hydrophobic region, namely EJh-M1 and EJh-L1M1, permeabilized the membranes to solutes with Stokes radii of about 6 Å (36, 37) in a lipid composition-independent fashion. This assay allows the assignment of the membrane lesion activity to the N-terminal hydrophobic region but does not rule out the cooperation of EJh-M2 in the entire EJh molecule. In terms of the alternative models for the active oligomer displayed in Fig. 1*B*, the present data support a holin oligomer structure in which the pore lining is formed by EJh-M1 units (*top view b*). Interestingly, EJh-M1 does contain a proportion of polar amino acids large enough to be considered amphipathic, but its N terminus contains a cluster of aromatic residues that have been referred to as functional ion sinks (42, 43). Adoption of this model requires also the verification of the capacity of EJh-M1 to oligomerize. In this sense, the relief of the self-quenching of fluorescein-labeled EJh-L1M1 upon co-incorporation into membranes with nonfluorescent peptide verifies this hypothesis. In this context, it is worth emphasizing the low stability displayed by the oligomers, because both β-octyl glucoside and SDS treatments reversed their association.

To investigate the nature of the membrane lesions produced by holins, the conventional leakage used in activity screening is probably an inadequate model. On a conceptual basis, holins are believed to generate membrane discontinuities large enough to allow the passage of a peptidoglycan hydrolase, which for EJ-1 phage is a 36-kDa amidase exhibiting a monomer-to-dimer equilibrium (44, 45). Both pore sizing using encapsulation relief strategies and the topographic analysis by atomic force microscopy of lipid-peptide assemblies evidenced membrane lesions large enough to allow the passage of the amidase partner across the bilayer. Interestingly, the large lesions that concur with biological activity seem to result from the enlargement of smaller holes upon the dynamic bilayer deformations required for the attachment to the mica. Probably the treatment used in these *in vitro* experiments would not be operative enough in a cellular environment, but the differences in composition between prokaryote cytoplasm and periplasm ensures a variety of ways to accomplish the needed bilayer stress. The observed slit enlargement implies the generation of peptide-naked lipid edges as shown in the nascent pores made by streptolysin O (46) and, consequently, their contemplation in the original model of holin action. In this sense, transbilayer holin oligomers could be considered as seeds for membrane deformation events.

Acknowledgments—We thank E. Díaz, J. L. García, and P. García for advice and helpful discussions. We also thank Douglas Laurents for the careful reading of the manuscript and for grammar corrections.

REFERENCES

1. Young, R. (1992) *Microbiol. Rev.* **56,** 430–481
2. Young, R., and Bläsi, U. (1995) *FEMS Microbiol. Rev.* **17,** 191–205
3. Wang, I. N., Smith, D. L., and Young, R. (2000) *Annu. Rev. Microbiol.* **54,** 799–825
4. De Ruyter, P. G., Kuipers, O. P., Meijer, W. C., and De Vos, W. M. (1997) *Nat. Biotechnol.* **15,** 976–979
5. Sanders, J. W., Venema, G., and Kok, J. (1997) *Appl. Environ. Microbiol.* **63,** 4877–4882
6. Gindreau, E., and Lonvaud-Funel, A. (1999) *FEMS Microbiol. Lett.* **171,** 231–238
7. Bläsi, U., and Young, R. (1996) *Mol. Microbiol.* **21,** 675–682

8. Steiner, M., and Bläsi, U. (1993) *Mol. Microbiol.* **8,** 525–533
9. Bläsi, U., Fraisl, P., Chang, C.-Y., Zhang, N., and Young, R. (1999) *J. Bacteriol.* **181,** 2922–2929
10. Raab, R., Neal, G., Garrett, J., Grimaila, R., Fusselman, R., and Young, R. (1986) *J. Bacteriol.* **167,** 1035–1042
11. Johnson-Boaz, R., Chang, C.-Y., and Young, R. (1994) *Mol. Microbiol.* **13,** 495–504
12. Zagotta, M. T., and Wilson, D. B. (1990) *J. Bacteriol.* **172,** 191–205
13. Smith, D. L., Struck, D. K., Scholtz, J. M., and Young, R. (1998) *J. Bacteriol.* **180,** 2531–2540
14. Díaz, E., Munthali, M., Lünsdorf, H., Höltje, J.-V., and Timmis, K. N. (1996) *Mol. Microbiol.* **19,** 667–681
15. Wellings, D. A., and Atherton, E. (1997) *Methods Enzymol.* **289,** 44–67
16. Alewood, P., Alewood, D., Miranda, L., Love, S., Meutermans, W., and Wilson, D. (1997) *Methods Enzymol.* **289,** 14–29
17. Rapaport, D., and Shai, Y. (1992) *J. Biol. Chem.* **267,** 6502–6509
18. Fominaya, J., Gasset, M., García, R., Roncal, F., Albar, J. P., and Bernad, A. (2000) *J. Gene Med.* **2,** 455–464
19. Bartlett, G. R. (1959) *J. Biol. Chem.* **234,** 466–467
20. Gasset, M., Saiz, J. L., Laynez, J., Sanz, L., Gentzel, M., Töpfer-Petersen, E., and Calvete, J. J. (1997) *Eur. J. Biochem.* **250,** 735–744
21. Goormaghtigh, E., Cabiaux, V., and Rysschaert, J. M. (1994) *Subcell. Biochem.* **23,** 329–362
22. Fringeli, U. P., and Günthard, H. H. (1981) *Mol. Biol. Biochem. Biophys.* **31,** 270–332
23. Bechinger, B., Ruysschaert, J.-M., and Goormaghtigh, E. (1999) *Biophys. J.* **76,** 552–563
24. Marsh, D. (1997) *Biophys. J.* **72,** 2710–2718
25. Ellens, H., Bentz, J., and Szoka, F. C. (1995) *Biochemistry* **24,** 3099–3106
26. Ladhokin, A. S., Selsted, M. E., and White, S. H. (1997) *Biophys. J.* **72,** 1762–1766
27. Jass, J., Tjarnhage, T., and Puu, G. (2000) *Biophys. J.* **79,** 3153–3163
28. Schneider, J., Dufrene, Y. F., Barger, W. R., Jr., and Lee, G. U. (2000) *Biophys. J.* **79,** 1107–1118
29. Tyrrel, J. W., and Attard, P. (2001) *Phys. Rev. Lett.* **87,** 17614–17616
30. Lindblom, G., Rilfors, L., Hauksson, J. B., Brentel, I., Sjolund, M., and Bergenstahl, B. (1991) *Biochemistry* **30,** 10938–10940
31. Strickland, E. H. (1974) *CRC Crit. Rev. Biochem.* **2,** 113–175
32. Woody, R. W. (1994) *Eur. J. Biophys.* **23,** 253–262
33. Aggeli, A., Boden, N., Chen, Y. L., Findlay, J. B., Knowles, P. F., Kovatchev, P., and Turnbull, P. J. (1996) *Biochemistry* **35,** 16213–16221
34. Hunt, J. F., Earnest, T. N., Bousché, O., Kalghatgi, K., Rielly, K., Horváth, C., Rothschild, K., and Engelman, D. (1997) *Biochemistry* **36,** 15156–151760
35. Ding, F. X., Xie, H., Arshva, B., Beckert, J. M., and Naider, F. (2001) *Biochemistry* **40,** 8945–8954
36. Bohrer, M. P., Deen, W. M., Robertson, C. R., Troy, J. L., and Brenner, B. M. (1979) *J. Gen. Physiol.* **74,** 583–593
37. Parente, R. A., Nir, S., and Szoka, F. C., Jr. (1990) *Biochemistry* **29,** 8720–8728
38. Rinia, H. A., and de Kruijff, B. (2001) *FEBS Lett.* **504,** 194–199
39. Young, R. (2002) *J. Mol. Microbiol. Biotechnol.* **4,** 21–36
40. Gründling, A., Bläsi, A., and Young, R. (2000) *J. Biol. Chem.* **275,** 769–776
41. Boden, N., Cheng, Y., and Knowles, P. F. (1997) *Biophys. Chem.* **65,** 205–210
42. Ladhokin, A. S., Selsted, M. E., and White, S. H. (1997) *Biophys. J.* **72,** 794–805
43. Corbin, J., Methot, N., Wang, H. H., Baezinger, J. E., and Blanton, M. P. (1998) *J. Biol. Chem.* **273,** 771–777
44. Saíz, J. L., López-Zumel, C., Monterroso, B., Varea, J., Arrondo, J. L., Iloro, I., García, J. L., Laynez, J., and Menéndez, M. (2002) *Protein Sci.* **11,** 1788–1799
45. Fernández-Tornero, C., García, E., López, R., Jiménez-Gallego, G., and Romero, A. (2002) *J. Mol. Biol.* **321,** 163–173
46. Palmer, M., Harris, R., Freytag, C., Kehoe, M., Tranum-Jensen, J., and Bhakdi, S. (1998) *EMBO J.* **17,** 1598–1605

Reconstitution of Holin Activity with a Synthetic Peptide Containing the 1–32 Sequence Region of EJh, the EJ-1 Phage Holin

Amparo Haro, Marisela Vélez, Erik Goormaghtigh, Santiago Lago, Jesús Vázquez, David Andreu and Mari?a Gasset

J. Biol. Chem. 2003, 278:3929-3936.
doi: 10.1074/jbc.M211334200 originally published online December 2, 2002
